AFWAL-TR-87-4038
ADA 181548

EFFECT OF FREQUENCY ON FATIGUE CRACK GROWTH RATE OF INCONEL 718 AT HIGH TEMPERATURE

TUSIT WEERASOORIYA

UNIVERSITY OF DAYTON
RESEARCH INSTITUTE
300 COLLEGE PARK DRIVE
DAYTON, OHIO 45469

JUNE 1987

INTERIM REPORT FOR PERIOD JANUARY 1984 THROUGH JANUARY 1987

MATERIALS LABORATORY
AIR FORCE WRIGHT AERONAUTICAL LABORATORIES
AIR FORCE SYSTEMS COMMAND
WRIGHT-PATTERSON AIR FORCE BASE, OHIO 45433-6533

NOTICE

When Government drawings, specifications, or other data are used for any purpose other than in connection with a definitely Government-related procurement, the United Stated Government incurs no responsibility or any obligation whatsoever. The fact that the Government may have formulated or in any way supplied the said drawings, specifications, or other data, is not to be regarded by implication, or otherwise in any manner construed, as licensing the holder, or any other person or corporation; or as conveying any rights or permission to manufacture, use, or sell any patented invention that may in any way be related thereto.

This report has been reviewed by the Office of Public Affairs (ASD/PA) and is releasable to the National Technical Information Service (NTIS). At NTIS, it will be available to the general public, including foreign nations.

This technical report has been reviewed and is approved for publication.

THEODORE NICHOLAS
Metals Behavior Branch
Metals and Ceramics Division

ALLAN W. GUNDERSON
Tech Area Manager
Metals Behavior Branch
Metals and Ceramics Division

FOR THE COMMANDER

JOHN P. HENDERSON, CHIEF
Metals Behavior Branch
Metals and Ceramics Division

If your address has changed, if you wish to be removed from our mailing list, or if the addressee is no longer employed by your organization please notify AFWAL/MLLN , W-PAFB, OH 45433- 6533 to help us maintain a current mailing list.

Copies of this report should not be returned unless is required by security considerations, contractual obligations, or notice on a specific document.

Unclassified

SECURITY CLASSIFICATION OF THIS PAGE

REPORT DOCUMENTATION PAGE

1a. REPORT SECURITY CLASSIFICATION Unclassified	1b. RESTRICTIVE MARKINGS
2a. SECURITY CLASSIFICATION AUTHORITY	3. DISTRIBUTION/AVAILABILITY OF REPORT Approved for public release; distribution is unlimited
2b. DECLASSIFICATION/DOWNGRADING SCHEDULE	
4. PERFORMING ORGANIZATION REPORT NUMBER(S)	5. MONITORING ORGANIZATION REPORT NUMBER(S) AFWAL-TR-87- 4038
6a. NAME OF PERFORMING ORGANIZATION University of Dayton Research Institute 6b. OFFICE SYMBOL (If applicable)	7a. NAME OF MONITORING ORGANIZATION Materials Laboratory (AFWAL/MLLN) Air Force Wright Aeronautical Laboratories
6c. ADDRESS (City, State and ZIP Code) 300 College Park Drive Dayton, Ohio 45469	7b. ADDRESS (City, State and ZIP Code) Wright-Patterson Air Force Base, Ohio 45433-6533
8a. NAME OF FUNDING/SPONSORING ORGANIZATION 8b. OFFICE SYMBOL (If applicable)	9. PROCUREMENT INSTRUMENT IDENTIFICATION NUMBER F33615-84-C-5051
8c. ADDRESS (City, State and ZIP Code)	10. SOURCE OF FUNDING NOS. PROGRAM ELEMENT NO.: 61102F; PROJECT NO.: 2307; TASK NO.: P1; WORK UNIT NO.: 18
11. TITLE (Include Security Classification) Effect of Frequency on Fatigue Crack Growth Rate of Inconel 718 at High Temperature	
12. PERSONAL AUTHOR(S) Tusit Weerasooriya	
13a. TYPE OF REPORT Interim	13b. TIME COVERED FROM 1/84 TO 1/87
14. DATE OF REPORT (Yr., Mo., Day) June 1987	15. PAGE COUNT 40
16. SUPPLEMENTARY NOTATION	

17. COSATI CODES		
FIELD	GROUP	SUB. GR.
14	02	
11/20	06/11	

18. SUBJECT TERMS (Continue on reverse if necessary and identify by block number)
Fatigue crack growth, time-dependent growth, cyclic-dependent growth, nickel-base superalloy, crack growth rate model, frequency effects.

19. ABSTRACT (Continue on reverse if necessary and identify by block number)

Fatigue crack growth was studied at 650°C as a function of frequency for several ratios of minimum-to-maximum stress intensity (R), and for two values of maximum stress intensity factor (K_{max}). Crack lengths were monitored at low frequencies from compliance calculations based on crack mouth opening displacement measurements. At higher frequencies, crack length was measured using a d.c. electric potential system. It was found that fatigue crack growth rate can be characterized in three distinct frequency regions. These three regions represent fully cycle-dependent, mixed, and fully time-dependent crack growth behavior and each region can be modeled by a power law function. Observation of micro-mechanisms support the existence of these three different regions of crack growth.

20. DISTRIBUTION/AVAILABILITY OF ABSTRACT UNCLASSIFIED/UNLIMITED ☒ SAME AS RPT. ☐ DTIC USERS ☐	21. ABSTRACT SECURITY CLASSIFICATION Unclassified
22a. NAME OF RESPONSIBLE INDIVIDUAL Theodore Nicholas	22b. TELEPHONE NUMBER (Include Area Code) 255-2689 22c. OFFICE SYMBOL AFWAL/MLLN

DD FORM 1473, 83 APR EDITION OF 1 JAN 73 IS OBSOLETE.

Unclassified

SECURITY CLASSIFICATION OF THIS PAGE

FOREWORD

This work was supported by the Air Force Wright Aeronautical Laboratories, Materials Laboratory at Wright-Patterson Air Force Base under AF Contract F33615-84-C-5051 and was conducted within the laboratories of the Metals and Ceramics Division of the Materials Laboratory under the monitoring of Dr. T. Nicholas of AFWAL/MLLN. Dr. N. E. Ashbaugh of the University of Dayton Research Institute was the Principal Investigator of the contract. This work was conducted between the period January 1984 through January 1987.

TABLE OF CONTENTS

TABLE OF CONTENTS (Concluded)

LIST OF ILLUSTRATIONS

LIST OF TABLES

SECTION 1

INTRODUCTION

Turbine engine disks of nickel-base superalloys are subjected to cyclic stresses and thermal transients at elevated temperatures as a result of throttle excursions and thermal gradients [1]. These operations produce loading patterns that cover a range of frequencies, amplitudes, and waveshapes. The Air Force has recently introduced damage tolerance requirements for critical structural components such as turbine disks. It is important, therefore, to be able to predict the growth rate of fatigue cracks in disk materials under the appropriate loading and temperature histories experienced in engines. This can be accomplished through a systematic study of the influence of the individual loading variables and the possible interactions among them. In the development of any model, the governing microstructural mechanisms should provide guidance.

Rates and micro-mechanisms of crack growth in nickel-base superalloys are, in general, a function of the maximum stress intensity factor (K_{max}), temperature (T), frequency (f), stress ratio (R), hold-time (t_H), waveshape, as well as material and microstructure. If all the variables except K_{max} are held constant, then the crack growth rate for most nickel-base superalloys such as Inconel 718 can be correlated with stress intensity factor as the governing parameter [2,3,4,5,6,7,8,9]. The other variables can then be used as modifying parameters in

modeling the behavior. To fully characterize fatigue crack growth rate (FCGR) as a function of one of the above variables, experiments can be conducted with other variables held constant throughout the test.

Modeling the FCGR behavior and interpreting the changes in micro-mechanisms of crack growth reduce to determining the explicit relationships of the independent variables in the expressions

$$da/dN = F_1(K_{max}, T, f, R) \quad (1)$$

$$\text{micro-mechanism of growth} = F_2(K_{max}, T, f, R) \quad (2)$$

In this paper, rates and micro-mechanisms of fatigue crack growth were studied as a function of two independent variables, frequency and R, in Equations 1 and 2 at T = 650°C.

In air and vacuum, under low cycle fatigue conditions, crack growth rate as a function of frequency has been studied in detail by Solomon [10,11]. He identified the existence of three major frequency regimes in air. Under K-controlled LEFM conditions [12], the present author obtained similar results for Inconel 718 at 650°C. The results from this investigation and others [6,7] show that for a given K_{max}, FCGR decreases with increasing frequency. At higher frequencies, the growth rate approaches a constant value. It has also been observed that the

crack growth mechanism changes from intergranular to transgranular with increasing frequency.

SECTION 2

EXPERIMENTAL TECHNIQUE

2.1 OVERVIEW

Systematic studies of fatigue crack growth as a function of test variables generally involves large numbers of constant load tests leading to scatter from specimen to specimen. In this investigation, the growth rates were obtained at two K_{max} values for three R values in a range of five decades of frequencies using only two specimens to obtain the necessary experimental information for the investigation. To minimize possible closure effects on crack growth, relatively high stress intensity factors which lie in the mid-power law region of the FCGR versus K_{max} curves were selected. In designing the experiments, the fact that the growth rate could be correlated with a power law function of K_{max} was taken into consideration. The power-law FCGR function has been reported in literature and also observed in this laboratory under various frequencies and hold-time conditions [13]. The method of testing was different from that typically used, where the tests are conducted under constant loading conditions by using a specimen for each test condition. This testing approach facilitated the study of crack growth behavior over a range of five decades of frequencies.

2.2 SPECIMEN GEOMETRY AND MATERIAL

A series of FCGR tests were conducted on Inconel 718 nickel-base superalloy. Tests were conducted using standard (ASTM E647) [14] C(T) specimens having a width, W of 40 mm and a thickness, B of 10 mm. To make the d.c. potential measurement of crack length, two Inconel 718 metal rods were welded to the C(T) specimen for the connection of the d.c. current supply. Leads for the d.c. electric potential measurements were spot-welded across the crack mouth. A diagram of the C(T) specimen with d.c. current rods is shown in Figure 1. Note also the location of the two holes which accepted the ends of the quartz rods attached to the extensometer used for compliance measurements.

All specimens were fabricated from the same heat of material. The heat treatment and composition of the IN718 material are shown in Table 1.

2.3 TEST CONDITIONS

All crack growth tests were conducted under constant stress intensity conditions. Two K_{max} values of 27.8 and 40 $MPa \cdot m^{1/2}$ were chosen to define the levels. Both these values lie in the mid-power law region of FCGR vs K_{max} curve. The tests were conducted over frequencies chosen from the range of 0.001 to 50 Hz and at a temperature of 650°C. Three different R ratios,

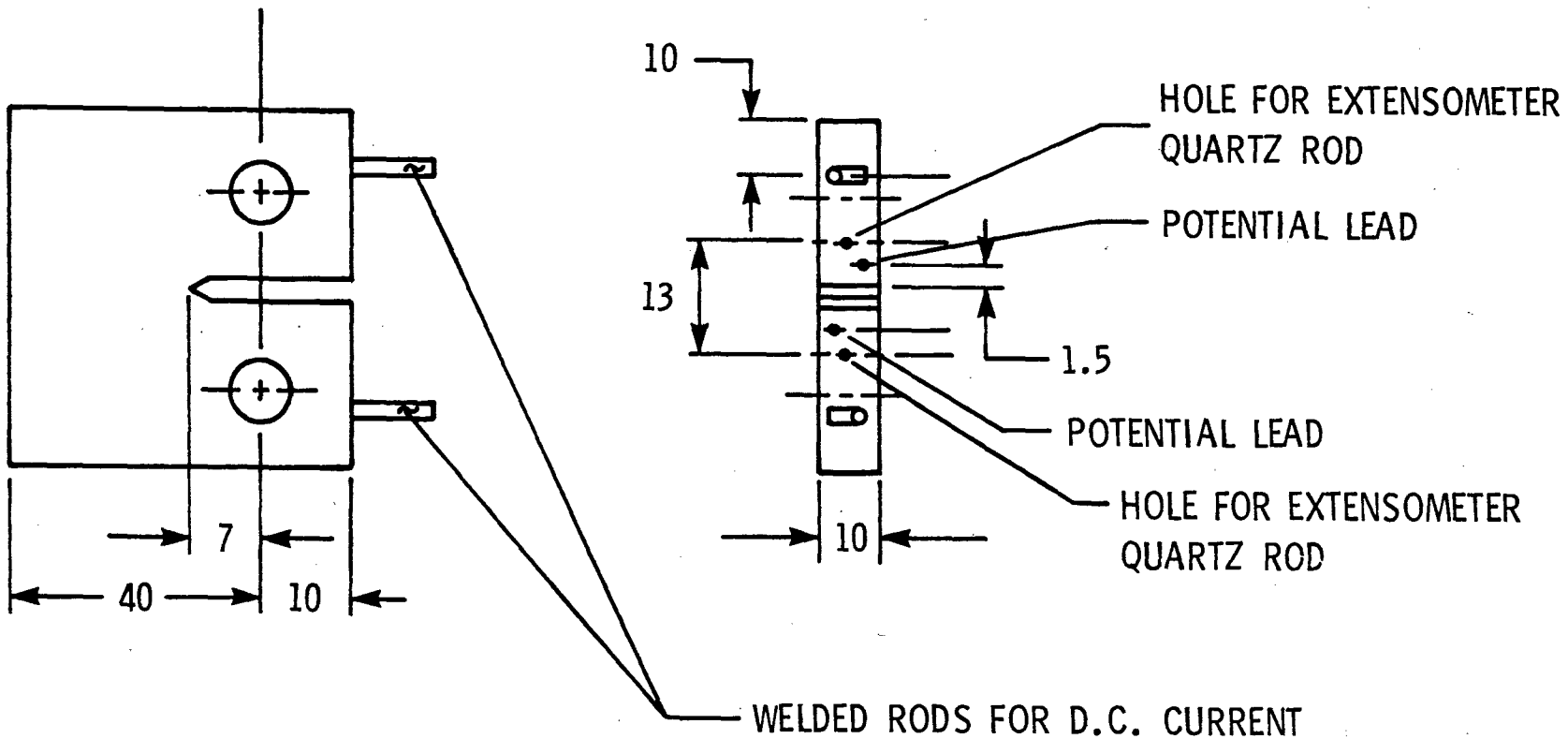

NOTES:

1. SPECIMENS FROM 0.5 INCH PLATE MATERIAL
2. CRACK ORIENTATION: TL
3. DIMENSIONS IN mm

Figure 1. The C(T) Specimen Modified for DC Potential and Displacement Measurements.

TABLE 1

CHEMICAL COMPOSITION BY WEIGHT AND HEAT TREATMENT FOR INCONEL 718

Ni	50-55	Cr	17-21
Fe	BAL.	Nb+Ta	4.75-5.5
Mo	2.8-3.3	Ti	0.65-1.15
Al	0.2-0.8	Co	<1.0
C	<0.08	Mn	<0.35
Si	<0.35	Cu	<0.30
Ph	<0.015	S	<0.015
B	<0.006		

HEAT TREATMENT

Step 1: Anneal at 968°C (1775°F) for 1 Hr., Air Cool to 718°C (1325°F).

Step 2: Age Harden at 718°C (1325°F) for 8 Hrs., Then Furnace Cool at 56°C/Hr. (100°F/Hr.) to 621°C (1150°F).

Step 3: Age Harden at 621°C (1150°F) for an Additional 8 Hrs.

Step 4: Air Cool to Room Temperature.

0.1, 0.5, and 0.8 were used in these experiments. A triangular loading waveform was utilized in all of the tests.

Specimens were precracked at 650°C to a crack length given by the ASTM E647 Standard (a = 10 mm) by applying a constant stress intensity that was less than the stress intensities used in the experiments.

2.4 TEST SYSTEM

An automated test system based on a microcomputer was employed in conducting these experiments. An electro-hydraulic servo-controlled test station with a 25 KN load cell was used to apply loading during the course of these tests. The microcomputer was used in real-time for feedback control of the test parameters and also to acquire and reduce data. The specimen was heated with a resistance furnace, and the temperature at a point on the specimen was controlled at 650±2°C. The temperature variation along the crack path was noted to be less than 10°C.

2.5 MEASUREMENT OF CRACK LENGTH

Crack length was measured in the range of frequencies between 10^2 and 10^{-3} Hz, using a hybrid crack measuring system. In this system, crack lengths were measured by both compliance and d.c. electric potential techniques. During testing, K_{max}

control was accomplished in different frequency ranges using one of the two techniques. Due to the inability of the extensometer to track the displacement correctly, the d.c. electric potential technique was used exclusively at high frequencies (f > 1.0 Hz). For lower frequencies (f <=1.0 Hz), controlling crack lengths were determined by the compliance technique. For the f <=1.0 Hz case, the d.c. electric potential crack length data were also collected for later evaluation of their accuracy and long term stability under the effect of environment at very low frequencies. Acquisition of load and displacement (compliance) data from the specimen to the microcomputer was accomplished using a digital oscilloscope. Electric potential data acquisition from the test machine to the microcomputer was performed utilizing a digital voltmeter.

The crack length was estimated at periodic cycle intervals chosen by the operator. The cycle interval was chosen to give a crack length increment less than 0.025 mm. After the crack length is determined using the stress intensity relationship given in ASTM E647 [14], the new load that is necessary to keep the K_{max} constant is determined by the computer software to within $\pm$ 0.1%. This computed load was then set up at the function generator through the IEEE-488 interface.

2.5.1 Compliance Method

During the test, crack length was determined indirectly from compliance measurements using displacement data obtained with a high temperature extensometer having quartz extension rods. With these quartz rods, the extensometer was maintained at ambient temperature since it was kept outside the furnace. Displacement and load data obtained simultaneously in digital form with the oscilloscope were transferred to the computer through an IEEE-488 interface bus. A straight line was fitted to a selected set of data chosen by a specified load window, using a least-squares error minimization procedure. Compliance that was obtained from the fitted straight line was converted to crack length using a relationship obtained by Saxena and Hudak [15] given in Equation 3, where C is the compliance, E is the modulus, B is the thickness of the specimen, and b = a/W.

$$CEB = (1+0.25/b)[(1+b)/(1-b)]^2.\{1.61369+12.6778b -14.2311b^2-16.6102b^3+35.0499b^4-14.4943b^5\}. \quad (3)$$

2.5.2 Electric Potential Method

Using the d.c. electric potential technique, crack length was determined at higher frequencies by measuring the potential across the crack tip at a constant d.c. current of 10 A. The constant current was generated by a stable power supply while the potential was measured by the voltmeter. Both

the power supply and the voltmeter were attached to the computer through the IEEE-488 bus. Using these instruments and the developed software, data were acquired and test conditions were controlled. To eliminate the thermal e.m.f., the potential data were also obtained at zero current. The electric potential data were acquired a given number of times at the upper one-third of a predefined number of successive cycles. The thermal e.m.f. adjusted average value of the potential was then converted to a crack length using an experimentally determined calibration curve.

2.5.3 Correction for Apparent Changes in Crack Length

It was observed that whenever f, K_{max}, or R was changed, the crack length estimated by the compliance method changed. The change in compliance estimated crack length occurred immediately after the change in external parameters and was not associated with any real change in crack length. Rather than continuing to use the newly estimated crack length that was established after the change, a procedure was developed to ensure continuity in crack length before and after the change in loading parameters. In essence, the procedure involved modifying the apparent elastic modulus after each change in loading parameters, so that the crack length before and after the change remained the same based on Equation 3.

2.6 TEST PROCEDURE

Using a triangular waveform, tests were conducted using two different procedures. In one test series, the temperature and R were held constant while the crack was grown for periods at various frequencies. In the other test category, while the frequency and temperature were held constant, the crack was grown for periods at different R values. Frequency and R sequences were selected to make distinct markings on the fracture surface. These marks were later used in verifying the crack lengths measured by d.c. potential and compliance methods. Figure 2 provides an example of a fracture surface from the tests. After fracture, each specimen was prepared for observation under optical and scanning electron microscope to determine the mechanisms of crack growth.

2.7 GROWTH RATE MONITORING

At the beginning of the test, the frequency and R sequence for the specimen was input to the computer. After each growth segment of 0.75 mm, either the frequency or R was automatically changed as specified. While the test was being conducted, the crack length as a function of the number of cycles was monitored by the operator on a graphical display. Crack growth rates derived from a linear regression representation of the data over the region where constant growth rate was observed were also displayed. With the aid of this real-time display of data, the

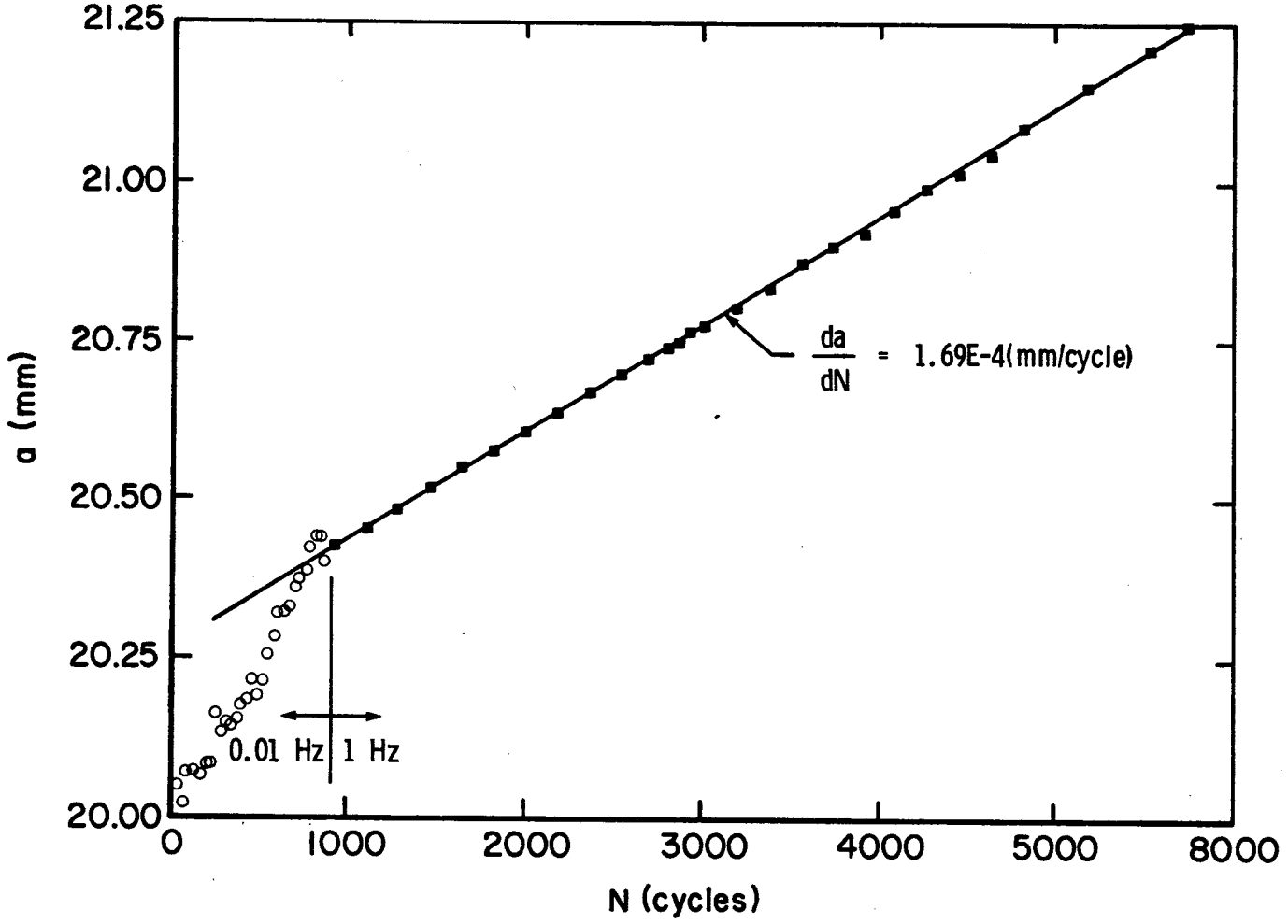

Figure 2. Fractured Specimens of Inconel 718 Showing Different Cracking Regions Corresponding to Test Under Different Conditions.

FCGR were obtained within crack extensions as small as 0.5 mm for given combinations of frequency, temperature, R, and K_{max} values. The graphical display also helped the operator determine if the crack growth rate had reached a steady-state value. This sophisticated testing procedure made it possible to obtain large amounts of data within a short time with very few specimens. To check the variability of growth rate, the crack was grown at $f = 1$ Hz, $T = 650°C$, $R = 0.1$, and $K_{max} = 40$ MPa$\cdot m^{1/2}$ at various crack lengths in the specimens. The variability of the FCGR from specimen to specimen and location to location was observed to be within a scatterband of 10% from the mean value for a given set of f, R, T, and K_{max} [16].

SECTION 3

RESULTS AND DISCUSSION

3.1 GROWTH RATE-FREQUENCY PLOTS AT R = 0.1

Fatigue crack growth data were obtained for Inconel 718 alloy as a function of frequency at R = 0.1 and at a temperature of 650°C. Typical crack length vs cycle data with a fitted linear line are shown in Figure 3 for a given test condition (K_{max} = 27.8 MPa·$m^{1/2}$ and f = 1 Hz). FCGR data as a function of frequency, obtained by fitting a least square error linear regression line for the crack length versus cycles curves are shown in Figure 4 for the maximum stress intensity factors of 27.8 and 40 MPa.$m^{1/2}$ for R = 0.1 and T = 650°C. Also in this figure, FCGR data at 1 Hz in vacuum [17] at 650°C, and at 1 and 4 Hz in air at room temperature are given for both K_{max} values. In Figure 5, FCGR data for K_{max} = 40 MPa·$m^{1/2}$ are presented using a time basis, i.e., da/dt is described as a function of frequency.

In Figure 4, the da/dN versus frequency curves can be represented with three linear lines separated by frequencies f_{tm} and f_{mt}, with a continuous transition from one to the other. The curve representing K_{max} = 40 MPa·$m^{1/2}$ is discussed in detail in the proceeding paragraphs.

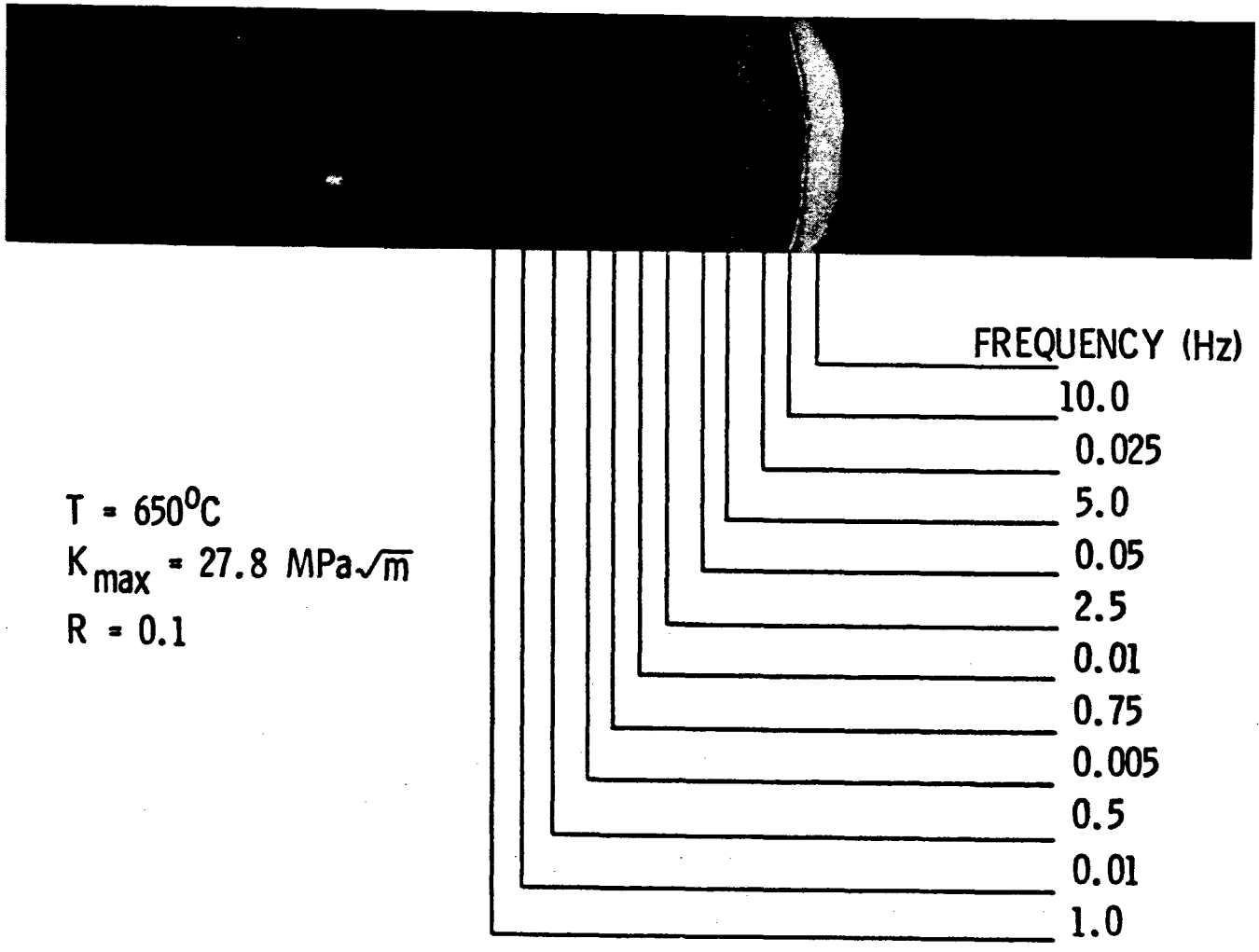

Figure 3. Typical a vs N Experimental Data with the Fitted Linear Regression Line.

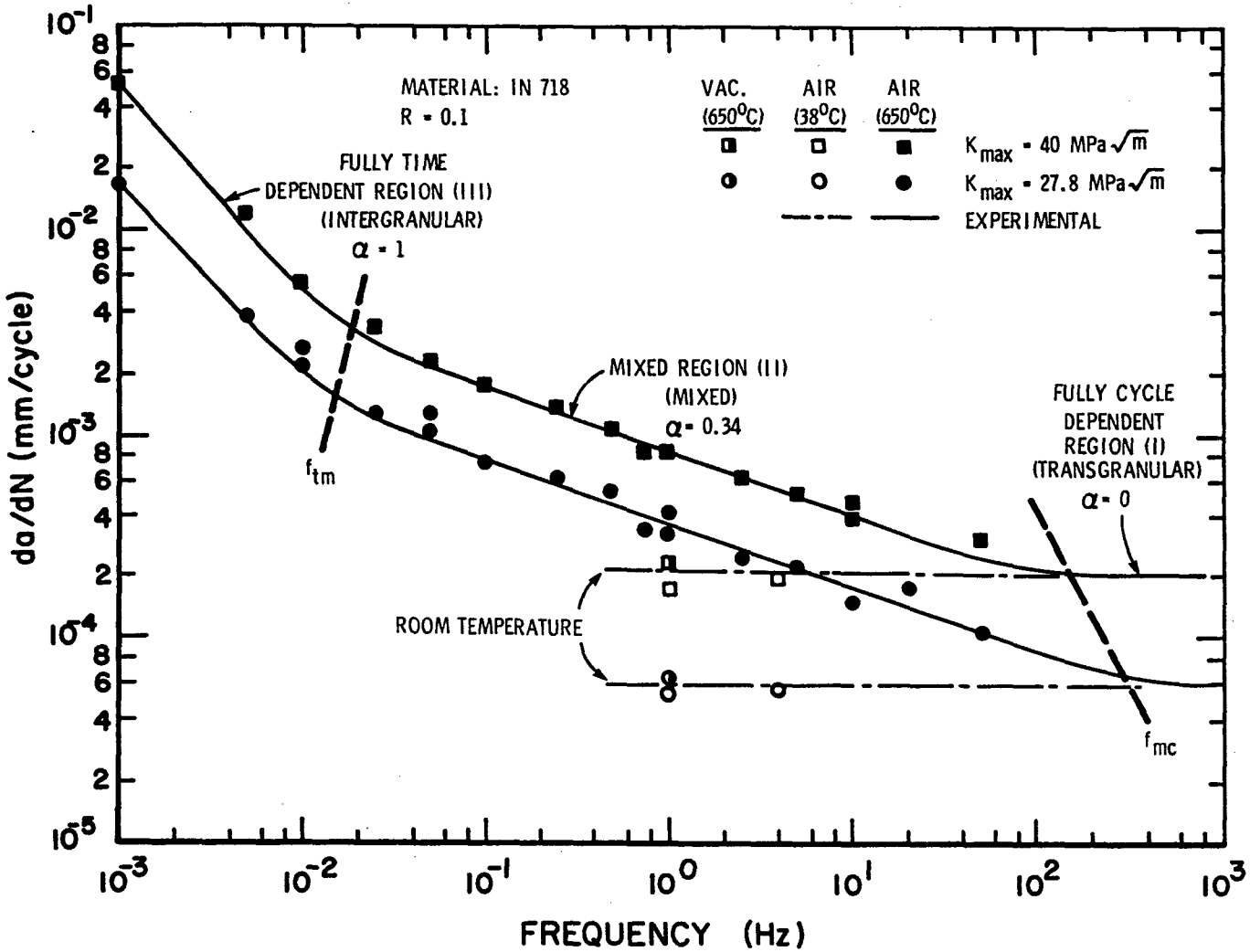

Figure 4. Fatigue Crack Growth Rate (da/dN) for Inconel 718 as a Function of Frequency at R = 0.1, Temperature = 650°C at Two Different K_{max} Values, 27.8 and 40 MPa·$m^{1/2}$. Also Data in Vacuum at 1 Hz [17] and Room Temperature Air Data are Given.

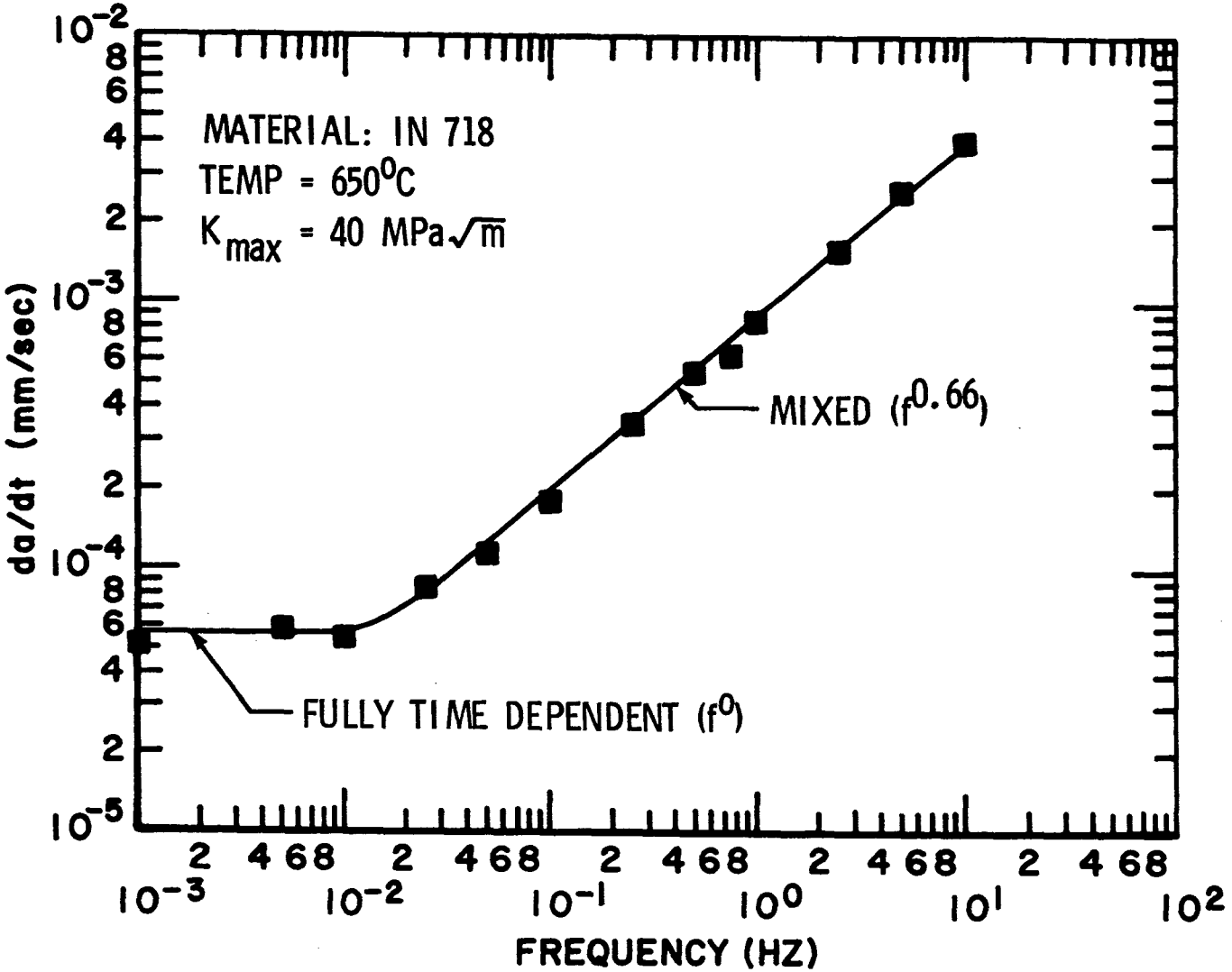

Figure 5. Time Rate of Crack Growth, (da/dt) for Inconel 718 as a Function of Frequency at K_{max} = 40 MPa·$m^{1/2}$, R = 0.1, and Temperature = 650°C.

3.1.1 Fully Time-Dependent Growth

In Figure 4, FCGR increases with decreasing frequency with a slope of -1 for the portion of the curve for frequencies below 0.01 Hz. This region represents fully time-dependent behavior where cycling has no effect on the growth rate based on time. The horizontal region of the da/dt curve in Figure 5 also illustrates the fact that the processes are fully time-dependent in this frequency regime. Under these conditions, time that is required to grow the crack a specific distance is a constant, and therefore, the factors determining the growth is independent of the number of cycles elapsed during that time. The damage is believed to occur by an environmentally enhanced rather than by a classical creep process.

3.1.2 Environmentally Enhanced Cycle-Dependent (Mixed) Growth

For frequency values between 0.01 and 10 Hz, log-log plots of da/dN versus frequency is linear with a slope of -0.34. In this middle frequency region, environment is affecting the cyclic damage and fracture is due to an environmentally enhanced fatigue process (mixed mode region).

3.1.3 Fully Cycle-Dependent Growth

Although there are not many data points at frequencies greater than 10 Hz for higher frequencies, da/dN is constant and should approach the frequency independent growth rate line at room temperature or high vacuum at 650°C. Though such a behavior was not specifically observed in air tests at 650°C, as we were unable to achieve ultra-high frequencies for the work reported in this paper, it was observed by Tien [18] that if the frequencies were sufficiently high, the effect of oxygen on the elevated temperature fatigue behavior could be suppressed resulting in a time-dependent but fully cycle-dependent process of damage. The asymptotic nature of the growth rate at higher frequencies was also proposed by Solomon and Coffin [11]. At frequencies greater than 50 Hz, fatigue crack growth is occurring so fast that there is insufficient time for environment to contribute to any damage at the crack tip. Hence, at very high frequencies, growth rates should approach the frequency independent growth rates at room temperature or in high vacuum at 650°C where there is no environmental damage. In this region, fracture at the crack tip is believed to occur under a pure cyclic plastic deformation process. In both cases, though there is no environmental damage at the crack tip due to oxidation, at room temperature, rewelding of the crack is prevented by the surface oxide film [19]. To establish the FCGR frequency behavior independent of environmental effects at 650°C, additional work is being conducted in vacuum [20].

3.2 EFFECT OF K_{max} ON FCGR-FREQUENCY PLOTS AT A GIVEN R (R = 0.1)

Fatigue crack growth rates as a function of frequency are shown in Figure 4 for maximum stress intensity factors of 27.8 MPa·$m^{1/2}$ and 40 MPa·$m^{1/2}$. Both of the stress intensity values in Figure 4 lie in the mid-power law region of the da/dN versus K_{max} curve as shown by Ashbaugh [9]. When K_{max} is 27.8 MPa·$m^{1/2}$, we also observed the existence of the above discussed three regions at 650°C. For the fully time-dependent region, da/dN is observed to be an inverse function of frequency, f, while for the mixed region, it is an inverse function of f^{α} (α = 0.34). At very high frequencies, that is in the fully cycle-dependent region, growth rates should approach a constant value, the room temperature growth rate, which is independent of the frequency and hence, the oxidizing environment. The slopes of the three regions of the da/dN versus frequency curves are seen to be reasonably independent of K_{max} for a given R value of 0.1 at 650°C for the two values of K_{max} chosen in this investigation. Also from Figure 4, as K_{max} increases, transition frequency from time-dependent to mixed regime increases and transition frequency from mixed to cycle-dependent decreases.

3.3 EFFECT OF R ON GROWTH RATE-FREQUENCY PLOTS AT $K_{max} = 40$ MPa·m$^{1/2}$

Tests were conducted at $K_{max} = 40$ MPa·m$^{1/2}$ for values of R = 0.1, 0.5, and 0.8. The purpose of these tests was to examine the effect of stress ratio on FCGR as a function of frequency. Observed FCGR data are shown in Figure 6. Also data in vacuum [17] at 1 Hz and in air at 650°C and room temperature, respectively, are presented in this figure for R = 0.1 and 0.5. At very high frequencies, FCGR is independent of frequency and should approach the growth rate at room temperature. All FCGR-frequency data in air at 650°C were characterized as falling within one of three regions: a fully time-dependent region with a slope of -1, a mixed region with a slope of -0.34, and a fully cycle-dependent region with a slope of zero. As R values were increased, the transition frequencies were shifted toward higher frequencies. Therefore, all three regions of crack growth were not observed for the high R values since some of the transition frequencies apparently fell outside the range of tested frequencies. In this study, for R = 0.5, only the fully time-dependent and mixed mode regions were observed. For R = 0.8, all data appeared to lie in the fully time-dependent region. For a given frequency, as R was increased, crack growth rate behavior tends to shift from a fully cycle-dependent mode to a mixed mode, and finally to a fully time-dependent mode. This behavior was expected since, as R was increased, the crack tip tends to be at

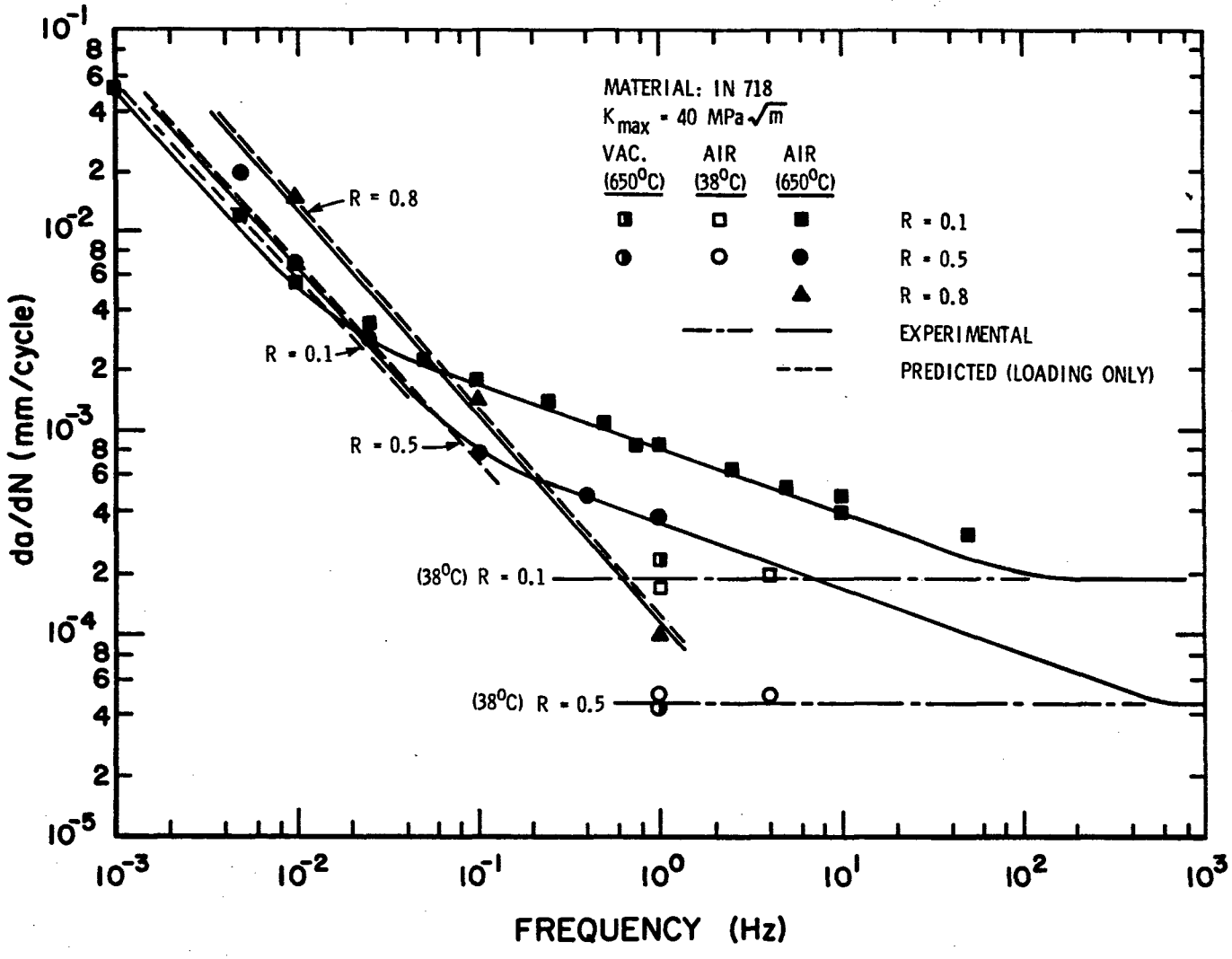

Figure 6. Fatigue Crack Growth Rate, (da/dN) for Inconel 718 as a Function of Frequency at K_{max} = 40 MPa·$m^{1/2}$ and Temperature = 650°C for Three Different R Values, 0.1, 0.5, and 0.8. Also 1 Hz Vacuum Data Points [17] and Room Temperature Data are Given for R = 0.1 and 0.5.

higher loads for a longer time for the same frequency, thus promoting environmentally enhanced damage at the crack tip.

3.4 TRANSITION FREQUENCIES

From Figures 4 and 6, the existence of transition frequencies from fully time-dependent to mixed fracture (f_{tm}), and from mixed fracture to fully cyclic-dependent fracture (f_{mc}), can be observed. Using these transition frequencies at a constant temperature, Equation 1 can be written in the form

$$(da/dN)_T = \frac{F_c(R,K_{max}) \cdot f_{mc}^{\alpha} \cdot f_{tm}^{(1-\alpha)} \cdot [1/f]}{[1+(f/f_{tm})^2]^{(1-\alpha)/2}[1+(f/f_{mc})^2]^{\alpha/2}} \qquad (4)$$

where $F_c(R,K_{max})$ is the fatigue crack growth rate as a function of K_{max} and R and room temperature and high frequency, and α corresponds to the negative slope of the mixed region of the fatigue crack growth rate versus frequency curves. Fatigue crack growth maps such as shown in Figure 4 and given in Equation 4, can be used to indicate transition frequency boundaries and FCGR behavior of three regions of fatigue crack growth [21].

3.5 MICRO-MECHANISMS OF CRACK GROWTH

Figure 7 shows typical fractographs taken from the three frequency regimes discussed above. An example of the fully cycle-dependent region is shown in Figure 7a. As shown, crack

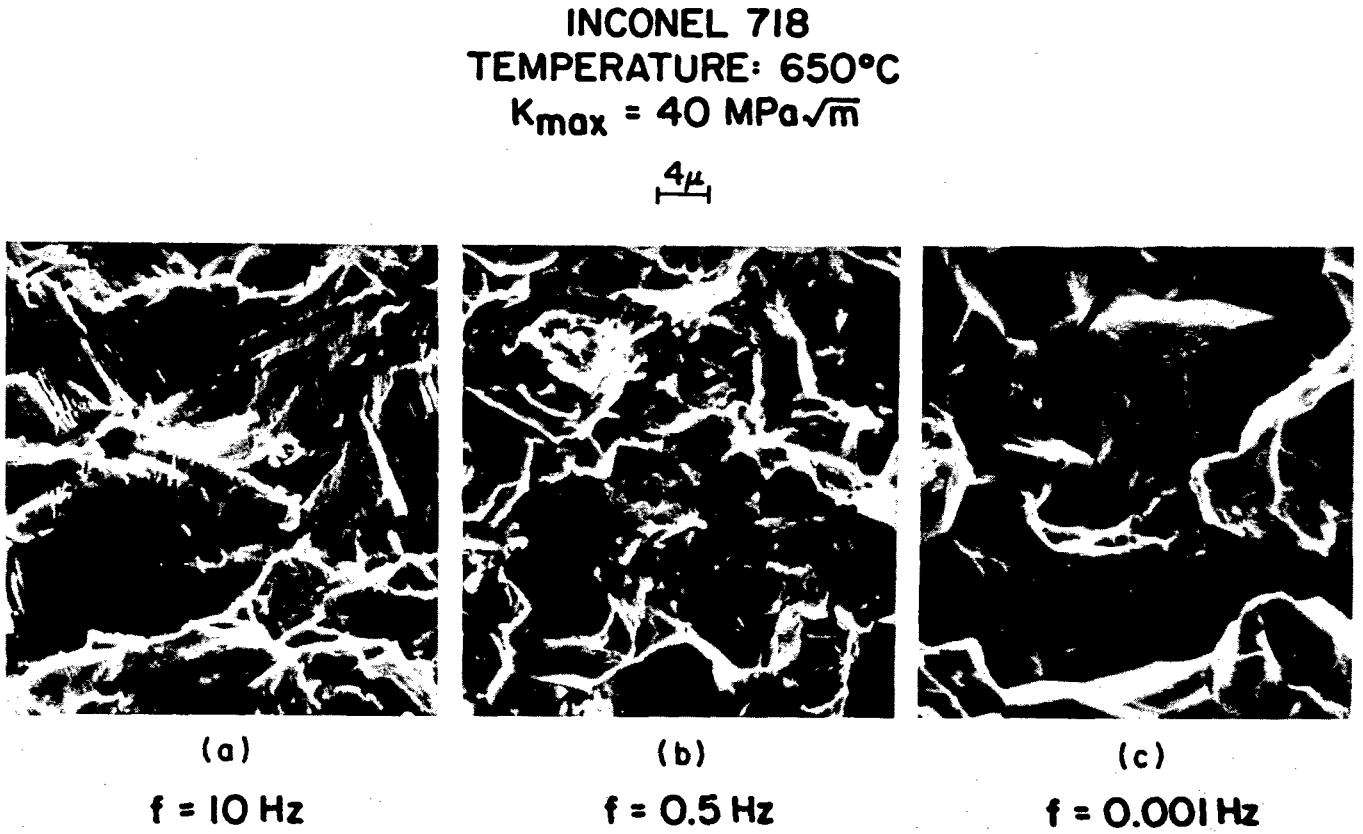

Figure 7. Scanning Electron Fractographs of Typical Fracture Surfaces for (a) Cycle-Dependent (10 Hz) Region, (b) Mixed (0.5 Hz) Region, and (c) Time-Dependent (0.001 Hz) Region. These Tests Were Conducted at 650°C, R = 0.1, and K_{max} = 40 MPa.$m^{1/2}$.

growth is caused by the formation of striations due to cyclic plastic deformation at the crack tip. A typical fracture surface taken from the mixed mode region is given in Figure 7b. In this case, a mixture of transgranular and intergranular fracture was observed. Figure 7c is a typical representation of fracture in the fully time-dependent region. In this region, cracking occurred only along the grain boundaries, and the total fracture surface was covered with grain boundary facets.

In general, as frequency was decreased, fracture morphology changed from pure transgranular to a mixture of transgranular-intergranular and finally to a fully intergranular mode independent of frequency, R, or K_{max}. These three frequency regimes that correspond to the observed changes in the fracture morphology are appproximately identical to the regimes that were detected from the changes in the slopes of FCGR-frequency curves discussed in previous sections for different values of R as well as K_{max} as shown in Figures 4 and 6.

3.6 MECHANISMS OF DAMAGE IN FULLY TIME-DEPENDENT REGIME

In the time-dependent region, crack growth occurred along the grain boundaries. Among the factors that could account for the time-dependent mechanisms are oxidation damage and creep-fatigue damage along the grain boundaries. Creep damage normally occurs by grain boundary cavitation and triple point cracking [22,23]. There was very little evidence of the presence of

either of these mechanisms. Thus, the environment appears to dominate the mechanism for damage under time-dependent conditions. There is evidence for this type of damage on the fracture surfaces; cracks were covered with oxides at lower frequencies. In general, oxygen can diffuse through grain boundaries faster than the bulk material at high temperatures. Environmental embrittlement of nickel-base superalloys at high temperature by oxygen penetration along the grain boundaries has been postulated in detail by Woodford and Bricknell [24]. In nickel-base superalloys, embrittlement is due to the penetration of gaseous species, primarily oxygen along the grain boundaries. Oxidation kinetics along the grain boundaries can be represented by an expression of the form

$$d = C \cdot t^{n} \cdot \exp(-Q/RT) \qquad (5)$$

where d is the depth of oxygen penetration, C, n, Q, and R are constants, T is temperature, and t is time [25]. But Equation 5 may not be applicable in modeling the grain boundary oxidation kinetics because the stress effects are not represented in the expression.

3.7 MODELING THE GROWTH BEHAVIOR

Phenomena of corrosion fatigue crack growth rate behavior (two regimes of pure cycle- and pure time-dependency in these cases) have been described in terms of linear superposition by

Gallagher and Wei [26], and Solomon and Coffin [11] for low cycle fatigue crack growth in vacuum at high temperature. As Solomon [10] has seen, crack growth rate data could not be expressed with a linear superposition model when the mixed regime is appreciably large. From Figures 4 and 6, FCGR at 650°C for a K_{max} in the mid-power law region of growth rate behavior and R values up to a maximum of 0.8 can be represented by the general expression

$$da/dN = MAX(F_c, F_m, F_t) \tag{6}$$

where F_c, F_m, and F_t are functions of R, f, and K_{max} which describe the FCGR behavior in the three frequency regimes, cycle-dependent, mixed, and time-dependent, respectively. In Equation 6, MAX function represents the maximum value of F_c, F_m, and F_t. The unified expression given in Equation 6 can be easily incorporated into a computer life prediction scheme, as almost all computer compilers have a built-in intrinsic MAX function. Separate prediction procedures of the above three functional expressions are discussed below.

3.7.1 Prediction of Growth Rates in the Fully Time-Dependent Region

A prediction was made of the cyclic crack growth rate under fully time-dependent behavior based solely on sustained load crack growth data. For this case, by integrating

the sustained load crack growth behavior during the total time period of the triangular waveform,

$$\frac{da}{dN} = 2\int_0^{\frac{1}{2}f} \frac{da}{dt}_s \cdot dt = 2C\int_0^{\frac{1}{2}f} [K(t)]^n \cdot dt \qquad (7)$$

where K(t) varies linearly with time for the triangular waveform and given by

$$K(t) = R.K_{max} + 2.K_{max}.(1-R).t.f \qquad (8)$$

f is the frequency, and $da_s/dt = C.K^n$ is the sustained load crack growth behavior of the material (n = 3). In Equation 7, da/dN represents the crack growth in one cycle. From substituting the triangular waveform relation for K(t) in Equation 7,

$$\frac{da}{dN} = \frac{C.K_{max}^{\ n}}{f} \cdot \frac{[1-R^{n+1}]}{(n+1)(1-R)} \qquad (9)$$

For the triangular waveform in the fully time-dependent region, the crack growth rates predicted by Equation 9 were approximately two times that of experimental data for a given frequency. Hence, for the triangular waveform in the fully time-dependent region, as shown in Figure 6, crack growth rate could be predicted by integrating the sustained load crack growth behavior along only the rising portion of the cycle. Dashed lines represent the predicted data from Equation 7 integrating only on the loading cycle of the waveform. This is consistent with the observations by Ashbaugh [9] who showed that under non-symmetric waveshape loading, the observed FCGR corresponds to

FCGR of the rising portion of the cycle only. But as R increases above 0.8, the cycling driving force, ΔK will be less than ΔK_{th} for this material. Assuming when $R > 0.8$ that the integration should be performed on the total period of the cycle, FCGR in the fully time-dependent regime is given by the expression

$$F_t(R,K_{max},f) = \frac{da}{dN} = \frac{C.K_{max}^{\ n}}{f} \cdot \frac{[1-R^{n+1}]}{(n+1)(1-R)} \cdot y \qquad (10)$$

where $y = 0.5$ for $(1-R)K_{max} \geq \Delta K_{th}$, and $y = 1.0$ for $(1-R)K_{max} < \Delta K_{th}$. An expression of this type would satisfy the limit condition, $R \rightarrow 1$, where $(da/dN).f$ should approach the sustained load crack growth rate, da/dt.

3.7.2 Prediction of Growth Rates in the Mixed Region

In the mixed region, FCGR was shown above to be proportional to $f^{-\alpha}$ for $R = 0.1$ and 0.5 at K_{max} of 40 $MPa \cdot m^{1/2}$, and for $R = 0.1$ at K_{max} of 27.8 $MPa \cdot m^{1/2}$. Using this observation, FCGR can be represented by the expression

$$F_m(R,K_{max},f) = da/dN = Cm \cdot R_m(R) \cdot (K_{max}^{\ nm}/f^{\alpha}) \qquad (11)$$

where Cm and nm are constants, and R_m is a function of R. If R_m is assumed to be of the Walker form [27,28]

$$R_m(R) = (1-R)^{mm} \qquad (12)$$

then mm could be evaluated from the data given in Figure 6 (mm = 1.50 and nm = 2.42). We were unable to verify this expression from the study reported in this report, as only two data points (R = 0.1 and 0.5) were available for any frequency chosen from the mixed regime. In future work, additional experiments will be conducted at other R values between 0.1 and 0.5 for more data points in this regime.

3.7.3 Prediction of Growth Rates in Fully Cycle-Dependent Region

In the fully cycle-dependent or environmentally-independent regime, FCGR is independent of the frequency. Also in this regime, the FCGR approaches a value given by a room temperature experiment as discussed earlier. Figure 8 shows the FCGR as a function of (1-R) for two K_{max} values, 27.8 and 40 $MPa \cdot m^{1/2}$ at room temperature. In this log-log plot, the variation of FCGR can be represented by straight lines for both K_{max} values where slopes of the two lines (mc) are identical, and mc = 2.14. In this frequency regime, FCGR can be represented by the expression

$$F_c(R,K_{max}) = da/dN = Cc \cdot (1-R)^{mc} \cdot K_{max}^{nc} \qquad (13)$$

where nc = 3.04.

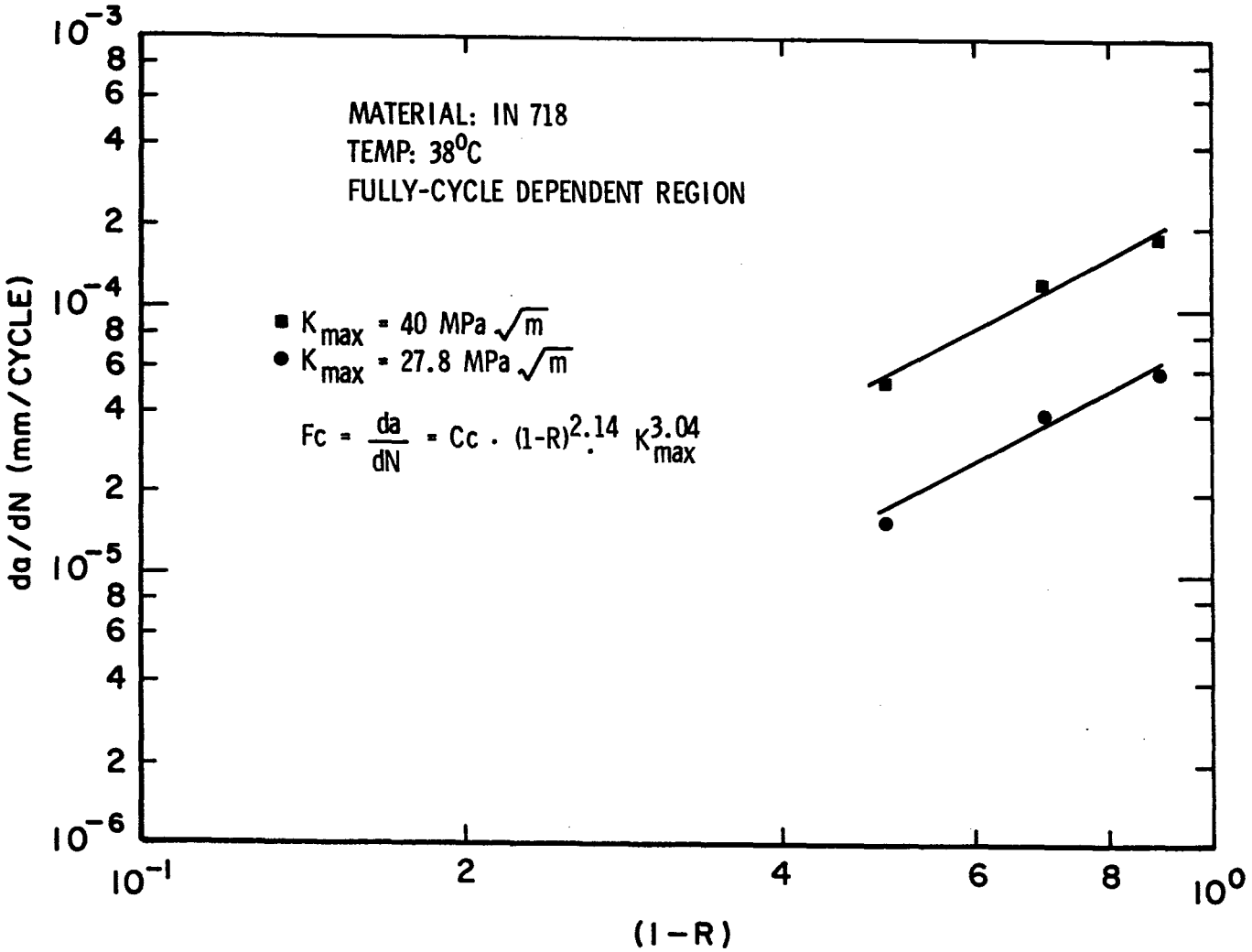

Figure 8. FCGR for Inconel 718 at Room Temperature (38°C) and 1 Hz as a Function of (1-R) for K_{max} = 27.8 and 40 MPa·$m^{1/2}$.

SECTION 4

CONCLUSIONS

At high temperatures, frequency dependence of fatigue crack growth rate can be divided into three modes of damage: fully cycle-dependent, mixed, and fully time-dependent damage, irrespective of R values, maximum stress intensity, and frequency. Three different models were derived for these frequency regimes which can be represented with a single function to get the overall crack growth rate under any condition of R, K_{max} (in the mid-power law regime) and frequency as shown in Equation 6. Micro-mechanisms of fatigue crack growth which were obtained from extensive fracture surface analysis also indicate the existence of these three regimes of damage, thus providing a physical basis for the above modeling.

REFERENCES

1. Larsen, J. M. and Nicholas, T., "Cummulative-Damage Modeling of Fatigue Crack Growth in Turbine Engine Materials," Engineering Fracture Mechanics, Vol. 22, No. 4, 1985, p. 713.

2. James, L. A., "Fatigue Crack Propagation Behavior of Inconel 718," HEDL Rep. TME 75-80, Hanford Engineering Development Laboratory, Westinghouse Hanford Company, Richland, Washington, September 1975.

3. Mills, W. J. and James, L. A., "Effect of Heat-Treatment on Elevated Fatigue-Crack Growth of Two Heats of Alloy 718," Paper 78-WA/PVP-3, American Society of Mechanical Engineers, New York, December 1978.

4. Clavel, M. and Pineau, A., "Fatigue Behavior of Two Nickel-Base Alloys I: Experimental Results on Low Cycle Fatigue, Fatigue Crack Propagation, and Substructures," Mat. Science and Engineering, Vol. 55, 1982, p. 157.

5. Pedron, J. P. and Pineau, A., "The Effect of Microstructure and Environment on the Crack Growth Behavior of Inconel 718 Alloy at 650°C Under Fatigue, Creep, and Combined Loading," Mat. Science and Engineering, Vol. 56, 1982, p. 143.

6. Clavel, M. and Pineau, A., "Frequency and Wave-Form Effects on the Fatigue Crack Growth Behavior of Alloy 718 at 293 K and 823 K," Met. Trans., Vol. 9A, 1978, p. 471.

7. Shahinian, P. and Sadananda, K., "Creep-Fatigue-Environment Interactions on Crack Propagation in Alloy 718," Engineering Aspects of Creep, Vol. 2, Paper C239/80, I. Mech. E., 1980.

8. Nicholas, T., Weerasooriya, T., and Ashbaugh, N. E., "A Model for Creep/Fatigue Interactions in Alloy 718," Fracture Mechanics: Sixteenth Symposium, ASTM STP 868, M. F. Kanninen and A. T. Hopper, Eds., American Society for Testing and Materials, Philadelphia, 1985, p. 167.

9. Ashbaugh, N. E., "Waveshape Effects Upon Crack Growth in Inconel 718," Presentation Given at 15th National Symposium on Fracture Mechanics, University of Maryland, College Park, Maryland, July 1982.

10. Solomon, H. D., "Frequency Dependent Low Cycle Fatigue Crack Propagation," Met. Trans., Vol. 4, 1973, p. 341.

11. Solomon, H. D. and Coffin, L. F., Jr., "Effect of Frequency and Environment on Fatigue Crack Growth in A286 at 1100°F," Fatigue at Elevated Temperature, ASTM STP 520, American Society for Testing and Materials, Philadelphia, 1973, p. 112.

12. Weerasooriya, T., "Effect of Frequency on Fatigue Crack Growth Rate at High Temperatures," Presentation Given at 16th National Symposium on Fracture Mechanics, Columbus, Ohio, August 1983.

13. Nicholas, T. and Weerasooriya, T., "Hold-Time Effects in Elevated Temperature Fatigue Crack Propagation," Fracture Mechanics: Seventeenth Volume, ASTM STP 905, J. H. Underwood, et. al, Eds., American Society for Testing and Materials, Philadelphia, 1986, p. 155.

14. Annual Book of ASTM Standards, Vol. 03.01, E647-86, American Society for Testing and Materials, Philadelphia.

15. Saxena, A. and Hudak, S. J., Jr., "Review and Extension of Compliance Information for Common Crack Growth Specimens," International Journal of Fracture, Vol. 14, No. 5, 1978, p. 453.

16. Weerasooriya, T. and Dirkes, E. M., "Variability of Fatigue Crack Growth Rate as a Function of Temperature, Frequency, and Stress Intensity Factor for Constant K Testing," Presentation Given at AIAA Mini-Symposium, Air Force Institute of Technology, Wright-Patterson Air Force Base, Ohio, March 1983.

17. Venkataraman, S., Nicholas, T., and Zawada, L. P., "Environmental and Closure Effects on the Fatigue Crack Growth Behavior of High Temperature Aircraft Alloys," Presentation Given at ASM Symposium - "Crack Propagation Under Creep and Creep-Fatigue", Orlando, Florida, October 1986.

18. Tien, J. K., "The Influence of Ultrasonic Frequency and Temperature on the Fatigue Behavior of a Nickel-Base Superalloy," Presentation Given at the 1971 American Institute of Mining, Metallurgical, and Petroleum Engineers' Meeting, 18 October 1971, Detroit, Michigan, Paper No. 12.

19. Tien, J. K. and Gamble, R. P., "The Room Temperature Fatigue Behavior of Nickel-Base Superalloy Crystals at Ultrasonic Frequency," Met. Trans., Vol. 2, 1971, p. 1933.

20. Venkataraman, S., Nicholas, T., and Weerasooriya, T., "Effect of Environment on Cycle- and Time-Dependent Crack Growth of IN718," Presentation Given at ASM Symposium - "Crack Propagation Under Creep and Creep Fatigue", Orlando, Florida, October 1986.

21. Weerasooriya, T., "Crack Growth Mechanism Maps for Inconel 718," Presentation Given at ASM Symposium - "Crack Propagation Under Creep and Creep-Fatigue", Orlando, Florida, October 1986.

22. Raj, R. and Ashby, M. F., "Intergranular Fracture at Elevated Temperature," Acta Met., 21, 1975, p. 1625.

23. Fields, R. J., Weerasooriya, T., and Ashby, M. F., "Fracture-Mechanisms in Pure Iron, Two Austenitic Steels, and One Ferritic Steel," Met. Trans., Vol. 11A, 1980, p. 333.

24. Bricknell, R. H. and Woodford, D. A., "The Embrittlement of Nickel Following High Temperature Air Exposure," Met. Trans., Vol. 12A, 1981, p. 425.

25. Yoshida, Y. and Liu, H. W., "Grain Boundary Oxidation and an Analysis of the Effects of Pre-Oxidation on Subsequent Fatigue Life," ASTM Symposium on Low Cycle Fatigue-Direction for the Future, 1985.

26. Gallagher, J. P. and Wei, R. P., "Crack Propagation Behavior in Steels," Proc. International Conference on Corrosion Fatigue: Chemistry, Mechanics, and Microstructure, 1972, p. 409.

27. Walker, K., "The Effect of Stress Ratio During Crack Propagation and Fatigue for 2024-T3 and 7075-T6 Aluminum," in Effects of Environment and Complex Load History on Fatigue Life, ASTM STP 462, American Society for Testing and Materials, Philadelphia, 1970, p. 1.

28. Coles, A., Johnson, R. E., and Popp, H. G., "Utility of Surface-Flawed Tensile Bars in Cyclic Life Studies," J. of Eng. Mat. and Technology, Vol. 98, 1976, p. 305.

U.S.Government Printing Office: 1987 — 748-061/60867